International Journal of Biological Macromolecules 321 (2025) 146214

Contents lists available at ScienceDirect

International Journal of Biological Macromolecules

journal homepage: www.elsevier.com/locate/ijbiomac

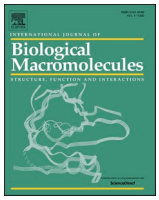

An optimal conversion cascading of distinct lignocelluloses to maximize bioethanol productivity and bio-adsorption capacities of Cd^{2+}/Cr(VI) and red/blue dyes selective for complete biomass recycling

Wenbo Yang [a,b,1], Boyang He [a,b,1], Hua Yu [a], Huiyi Zhang [a,b], Yunong Li [a,b], Jingyuan Liu [b], Hao Peng [a], Hailang Wang [a,b], Peng Liu [a], Yanting Wang [a], Liangcai Peng [a,b], Dan Sun [a,*]

[a] Key Laboratory of Fermentation Engineering (Ministry of Education), Cooperative Innovation Center of Industrial Fermentation (Ministry of Education & Hubei Province), Hubei Key Laboratory of Industrial Microbiology, School of Life & Health Sciences, School of Material Science & Chemical Engineering, Hubei University of Technology, Wuhan 430068, China

[b] College of Plant Science & Technology, Huazhong Agricultural University, Wuhan 430070, China

ARTICLE INFO

Keywords:
Lignocellulose
Biosorbent
Biochar

ABSTRACT

Although agriculture and forestry provide enormous lignocellulose resources, it remains to explore a novel technology for efficient biomass conversion into renewable bioethanol followed with complete recycling for valuable bioproduction with zero- waste release. As classic chemical (acid and alkali) pretreatments could cause chemical waste liberation, this study performed optimal pretreatments with hot-$FeCl_3$ for sequentially enhancing biomass enzymatic saccharification in three bioenergy crops, which led to achieving hexoses yields raised by 4–7 times compared to the controls. By employing engineered yeast strain for xylose co-fermentation, the highest bioethanol yield was achieved at 18 % (% dry matter) in *Miscanthus* sample. The remaining enzyme-undigestible residue was thermal-chemically converted into high-porosity biochar capable of upgraded organic dyes adsorption. The yeast-fermentation residue of wheat was further incubated with classic oxidative chemicals for desirable biosorbent assembly with the highest Cd^{2+} adsorption capacity (25 mg/g), whereas the fermentation residue of *Eucalyptus* was mixed with its pretreatment liquid to generate another optimal biosorbent for maximum Cr(VI) adsorption (20 mg/g) among all biosorbents (7–13 mg/g) examined to date. A novel hypothetic model is thus proposed about how distinct lignocelluloses are convertible and selectable for high-yield bioethanol and high-performance bioproducts, providing insights into the optimal lignocellulose utilization under green-like processes.

1. Introduction

Lignocellulose is the most abundant biomass resource that can be transformed into sustainable biofuels and valuable bioproducts [1–3]. In general, biomass sources are categorized into two types: crop straws harvested from agricultural cultivable lands and lignocellulose-rich plants grown in forestry margins [4,5]. Wheat is one of the major food crops having a large amount of lignocellulose residues, *Miscanthus* is a bioenergy crop that results in a high lignocellulose yield and adapts well to various marginal lands, and *Eucalyptus* has the advantages of intense lignocellulose productivity and rapid economic returns owing to its fast growth and short life cycle [6–9]. Although these three plant species provide distinct lignocellulose resources, the natural recalcitrance of lignocelluloses principally restricts cost-effective biomass saccharification, which is unacceptable in efficient biofuel conversion and bioproduct generation, and causes potential secondary waste release into the environment [10,11].

The recalcitrant property of lignocelluloses is principally affected by diverse plant-cell-wall compositions and characteristic wall-polymer features [12,13]. To reduce lignocellulose recalcitrance, physical and chemical pretreatments have been implemented by partially extracting non-cellulosic polymers (lignin and hemicellulose) and specifically reducing cellulose polymerization [14]. However, these pretreatments mostly require extreme conditions, such as high pressure, and expensive

* Corresponding author.
E-mail address: 80367532@qq.com (D. Sun).
[1] These authors contributed equally to this work.

https://doi.org/10.1016/j.ijbiomac.2025.146214
Received 25 September 2024; Received in revised form 15 July 2025; Accepted 20 July 2025
Available online 22 July 2025

equipment for physical processes and high concentrations of acids and alkalis for chemical processes; thus, costly and high-energy inputs are involved, and secondary chemical and biomass wastes may be produced [15,16]. To address these limitations, green-like pretreatments, such as nonchemical and recyclable chemical treatments, are increasingly being considered. For example, liquid hot water (LHW) has been applied in nonchemical biomass pretreatment, but its effectiveness is limited because of lignocellulose recalcitrance [17–19]. Recyclable chemicals ($FeCl_3$) have been used as active catalysts for effective wall-polymer extraction and disassociation, leading to near-complete biomass enzymatic saccharification in corn straws [20,21]. However, an optimal technology for cost-effective biomass processes with zero waste release needs to be explored.

Cellulosic ethanol is a perfect additive to petrol fuels and can be obtained via yeast fermentation with hexoses released from cellulose hydrolysis; however, the second-largest xylose resulting from hemicellulose digestion is not fermentable by the classic yeast strain [22,23]. Thus, engineered yeast strains are used for xylose–ethanol co-conversion to increase the yield of bioethanol [24,25]. The lignin-rich residue after yeast fermentation is considered to be a valuable bioproduct. For instance, lignocellulose-derived biosorbents are broadly employed in heavy metal elimination, whereas biochar materials can be generated by thermally and chemically converting lignocellulose substrates for multiple purposes [26]. Cd^{2+} and Cr(VI) are distinct heavy metals that pollute agricultural soils; thus, specific bio-absorbents suitable for the maximum adsorption of these heavy metals must be explored [27,28]. Moreover, methylene blue (MB) and Congo red (CR) are two industrial dyes that cause severe damage to human health; thus, chemically modified biochars are also considered for the efficient elimination of these dyes [26,29].

In this study, we collected distinct lignocellulose substrates from three major types of bioenergy crops (wheat, *Miscanthus*, and *Eucalyptus*) and performed an optimal LHW-$FeCl_3$ pretreatment to enhance biomass enzymatic saccharification. We employed our previously engineered yeast strain (E4/SF7-Ft3-X2), suitable for the co-conversion of hexoses and xylose, to achieve a high yield of bioethanol [25]. Furthermore, we integrated all solid residues from yeast fermentation with the supernatants of the LHW-$FeCl_3$ pretreatment to generate chemically modified biosorbents via a chemical (NaOH and H_2O_2) oxidation reaction. Interestingly, we determined that the chemically modified biosorbent of the *Eucalyptus* sample exhibited the highest Cr(VI)-adsorption capacity among all biosorbents generated in this study and previous studies. However, these biosorbents displayed low Cd-adsorption capacities. Thus, we generated other biosorbents by performing a chemical (NaOH and H_2O_2) oxidation reaction with only the fermentation residues, and the wheat sample showed the highest Cd-adsorption capacity among all biosorbents reported to date. We attempted to obtain biochar samples from classic thermal–chemical conversions using three lignocellulose sources: raw straws, enzyme-undigestible residues, and fermentation residues of bioenergy crops. Notably, we found that the enzyme-undigestible biochar residues of the *Miscanthus* sample had high adsorption capacities for two distinct dyes (MB and CR). Based on all the major findings obtained in this study, we finally developed a mechanistic model to elucidate how distinct lignocelluloses are selectable for high-yield bioethanol production and high-efficiency adsorption of diverse heavy metals and industrial dyes; this is a novel strategy for optimal biomass conversion and recycling under green-like processes.

2. Materials and methods

2.1. Preparation of biomass samples

Miscanthus and wheat plants were grown in the experimental fields of Huazhong Agricultural University and their mature straws were harvested in October 2021 and May 2022, respectively. *Eucalyptus* stem tissues were obtained from Guangxi Province. All lignocellulose tissues were dried at 50 °C, ground into powder through 40 mesh screen and stored in sealed dry container until in use (Fig. 1).

2.2. Wall polymer extraction and analysis

Plant cell wall fractionation was conducted to extract hemicelluloses and cellulose fractions as previously described [30,31]. Total hemicellulose was measured by calculating total hexoses and pentoses of the hemicellulose fraction and the pentoses of cellulose fraction. Total hexose of cellulose fraction was measured as cellulose level. All analyses were accomplished in independent biological triplicate.

2.3. Liquid hot water (LHW)-$FeCl_3$ pretreatment

Biomass samples (0.300 g) were supplied with 2.4 mL 4 % $FeCl_3$ (*w/v*), and well-mixed samples were placed into stainless steel bomb with PTFE jars and a thermostatic magnetic stirrer (Kerui Instrument Co., Ltd., Gongyi, China) under shaken at 60 rpm [21]. The sealed samples were incubated at 130 °C, 150 °C and 170 °C for 5 min, 10 min and 15 min, respectively. After the bombs were cooled to room temperature, the pretreated samples were rinsed several times with deionized water until pH 7.0, and the remaining solid residues were collected for enzymatic hydrolysis. All assays were carried out in independent triplicate.

2.4. Biomass enzymatic saccharification and yeast fermentation

The pretreated biomass samples were washed twice with 0.2 M phosphate buffer (pH 4.8), and then incubated with the final concentrations of 2 g/L mixed-cellulases (40 mg/g biomass) under 150 rpm shaken for 48 h at 50 °C and while co-supplied with 1 % Tween-80 as described [32]. After centrifugation at 3000 *g* for 5 min, the supernatants were collected for hexoses and pentoses as previously described [33]. For ethanol fermentation, commercial yeast strain (Angel, Angel yeast Co., Ltd., Yichang, China) and engineered yeast strain (E4) [25] were respectively incubated with the enzyme hydrates of pretreated lignocelluloses to final 6 mL solution of 0.5 g/L yeast concentration for 48 h under anaerobic conditions at 37 °C [34]. After fermentation, the ethanol yield was measured as previously described. All experiments were performed with independent biological triplicates.

2.5. Preparation of biosorbents and biochar samples

For biosorbents generation, three major types of lignocelluloses of bioenergy crops were prepared including raw straws, yeast fermentation residues mixed with pretreatment supernatants (FR-PS), and the fermentation residues only (FR) [26]. The samples of raw straws and fermentation residues were respectively washed with distilled water and dried in 50 °C through a 60 mesh for use, whereas the fermentation residues were mixed with pretreatment supernatants (1:20, w:v) and dry in 50 °C for use. All dried lignocellulose samples were respectively incubated with 20 mL chemicals (containing 1 % NaOH and 0.9 % H_2O_2) under 150 rpm shaken for 3 h at 50 °C, then transferred to 30 °C for 15 min, and cool to room temperature. The samples were then adjusted to pH 7.0 with 1.0 M HCl, and centrifuged for 5 min at 3000 *g* to collect solid residues. The residues were further washed with 75 % ethanol for 2–3 times and acetone once, and dried at 50 °C to constant weight as biosorbent samples.

For biochar generation, the lignocellulose samples were mixed with KOH (1:4, w:w), and ground into the powder [35]. The powders were loaded into a tube furnace (OTF-1200X-60UV, Kejing Material Technology Co., Ltd., Hefei, China) for heating under N_2 at a rate of 10 °C/min up to 300 °C for 1 h, and then at a rate of 5 °C/min to 800 °C to maintain for 2 h, and finally at a cooling rate of 10 °C/min to room temperature. The cooled materials were transferred to a 250 mL triangular flask and incubated with 150 mL 1 M HCl solution under stirring for 24 h with a magnetic stirrer thoroughly well-mixing. After removing

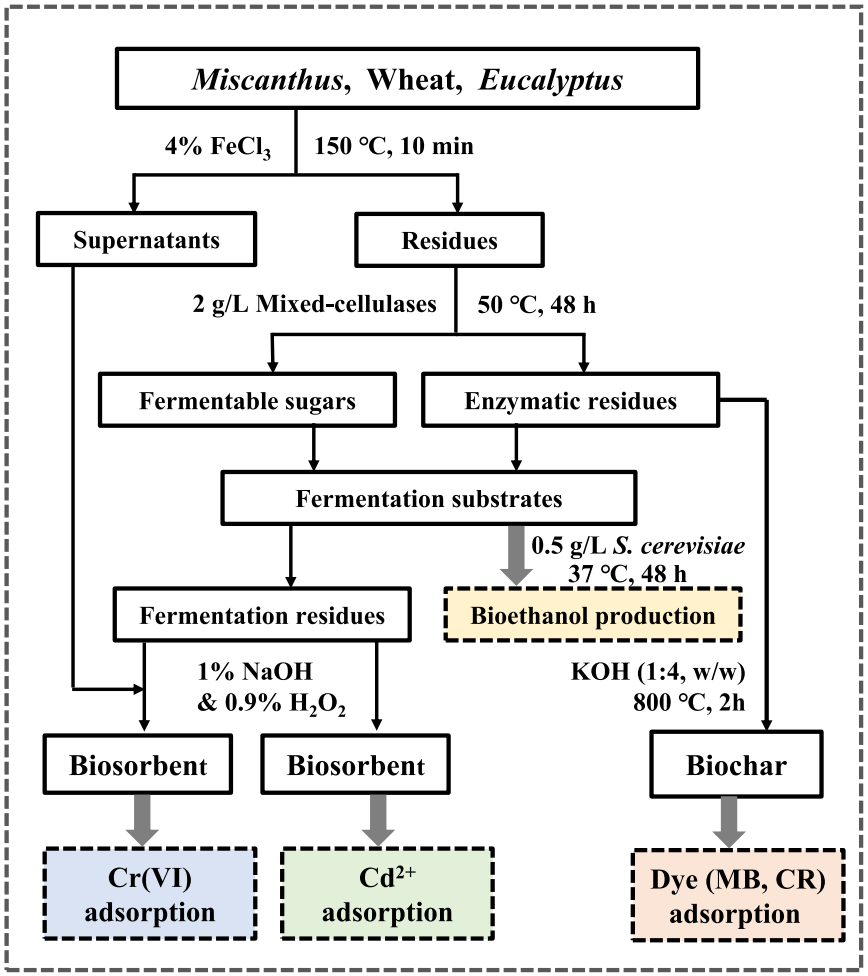

Fig. 1. Experimental flow chart for lignocellulose conversion into bioethanol followed with the solid residues and liquid supernatant selective for generations of biochar and biosorbents.

the supernatant, the solid residues were washed with 200 mL distilled water until pH 7.0, then repeatedly washed with anhydrous ethanol for final ultrasonic treatment at room temperature at 40 KHz for 12 h. After thoroughly mixing, and supernatant removal, the solid residues were precipitated at 60 °C and passed through 160 mesh sieve as biochar samples.

2.6. Heavy metals and organic dyes adsorption analyses

For biosorbent adsorption assay, 2 mg/L Cd^{2+} solution was prepared by adding $Cd(NO_3)_2{\cdot}4H_2O$ into ultrapure water, and to about 25 mL Cd^{2+} solution (pH 7.0) was added then added 0.025 g biosorbent with 1 g/L dosages, and then shaken at 150 rpm and 25 °C for 1 h. After adsorption reaction, the sample was centrifuged at 3000 *g* for 5 min, and the supernatant was collected and diluted to a standard curve range to measure Cd^{2+} by flame atomic adsorption spectrophotometer (FAAS HITA-CHI Z-2000, Tokyo, Japan) equipped with air-acetylene flame as described [36].

For Cr(VI) absorption assay, 0.1 g/L chromium standard storage solution was prepared by adding 0.2829 g of potassium dichromate $K_2Cr_2O_7$ (superior pure dried at 120 °C for 2 h) to 1000 mL distilled water. Two chromium standard solution (I) and (II) were then prepared: 5.0 mL and 25.0 mL of chromium standard stock solution into a 500 mL volumetric flask, diluted with distilled water to the mark, shaken well, and each milliliter of solution containing 1.00 μg and 5.00 μg hexavalent chromium as fresh use.

Color reagent was prepared by dissolving 0.2 g of diphenylcarbazide ($C_{13}H_4N_4O$) in 50 mL acetone, diluted with distilled water to 100 mL, shaken well, and stored in dark conditions. Standard curves for chromium solution were prepared to 50 mL with water in a 50 mL glass volumetric flask (g/mL). By adding 0.5 mL of sulfuric acid solution (1:1, v:v) and 0.5 mL of phosphoric acid solution (1:1, v:v), the solutions were shaken well, and then added with 2 mL color reagent for 10 min. Distilled water was used as a blank control to detect at 540 nm for a standard curve.

By adding 0.02 g biosorbent to 20 mL of Cr(VI) solution, the biosorbent sample was placed in a constant temperature oscillator, and the oscillation rate is 100 rpm for 24 h. After oscillation, the samples stand to collect the supernatants. After appropriate dilution, 2 mL supernatant, 20 μL Sulfuric acid solution (1:1, v:v), 20 μL Phosphoric acid solution (1:1, v:v) and 80 μL Color developer (DPCI) were mixed to read at 540 nm colorimetric.

The Cd/Cr(VI) adsorption capacity at equilibrium q_e (mg/g) and the percentage removal efficiency (% R) were estimated as previously described [37]. All assays were completed under independent triplicate.

For Congo Red (CR) adsorption assay, 0.025 g biochar was added into the different concentrations of CR solution (500 mg/L, 800 mg/L, 1000 mg/L, 1500 mg/L, 2000 mg/L and 2500 mg/L) in 25 mL tubes, mixed well and shaken under 150 rpm for 4 h at 25 °C. After centrifugation at 8000 *g*, the supernatants were collected to detect the remaining dyes level at 498 nm for measurement of the CR adsorption capacity and absorption rate (%).

For blue organic dye MB adsorption assay, 0.025 g biochar was added into the different concentrations of MB solution (600 mg/L, 800

mg/L, 1000 mg/L, 1200 mg/L, 1500 mg/L and 2000 mg/L) in 25 mL tubes, mixed well and shaken for 4 h under 150 rpm at 25 °C. Apart from analyzing different wavelength (λ_{max} = 664 nm), the analysis steps and calculation methods for MB were the same as those for CR. Langmuir isotherm and Freundlich isotherm models were characterized as described [35,38]. The linear form of the pseudo-second-order equation was plotted as described [36,39]. All assays were conducted at independent triplicate.

2.7. Characterization of biosorbents and biochar samples

The biochar samples were respectively characterized by X-ray diffraction (XRD, Advance D8), Raman spectrum (Thermo Scientific DXR, Waltham, MA, USA), scanning electron microscopy (SEM, Gemini 500, Obercohen, Germany) as previously described [35]. BET assay for specific surface area and pore diameter was accomplished by Automated Surface Area and Porosity Analyzer (Micromeritics ASAP 2460, Norcross, GA, USA). Lignocellulose chemical linkages were detected by Fourier transform infrared (FT-IR) method (Thermo Fisher Scientific, Waltham, MA, USA) as described [29]. The elements and binding energy of carbon materials were detected by X-ray photoelectron spectroscopy (XPS, Thermo Scientific K-Alpha, Waltham, MA, USA).

2.8. Statistical analysis

Analyses of variance (ANOVA), regression coefficients and Spearman's rank correlation coefficient were respectively accomplished using Superior Performance Software System (SPSS version 16.0, Inc., Chicago, IL). Pair-wise comparisons were conducted between two measurements by Student's *t*-test. The line graph, histogram, and regression analysis for the best fit curve were plotted using Origin 8.5 software (Microcal Software, Northampton, MA). The average values were calculated from the original independent triplicate measurements for these analyses.

3. Results and discussion

3.1. Optimal LHW-$FeCl_3$ pretreatments for enhanced biomass saccharification in three representative bioenergy crops

As agricultural crops of arable soils and fast-growing plants of marginal lands represent primary biomass resources, this study collected distinct lignocellulose substrates from three representative plant species: wheat, *Miscanthus*, and *Eucalyptus* (Table 1). In comparison, *Miscanthus* stalk is rich in cellulose and hemicellulose, *Eucalyptus* stems contain high proportions of cellulose and lignin, and wheat straw has relatively low cellulose and lignin levels with high hemicellulose content. Based on our previously established LHW-$FeCl_3$ pretreatment, we explored the optimal incubation time and temperature for the three lignocellulose substrates (Fig. S1). By measuring hexose yield released from enzymatic hydrolysis of pretreated lignocellulose, we identified the optimal pretreatment applicable for three bioenergy crops by incubating 4 % $FeCl_3$ with LHW at 150 °C for 10 min. The optimal LHW-$FeCl_3$ pretreatment increased the hexose yields (% cellulose) of the three bioenergy crops by 5–13 times compared with that of the raw biomass (Raw) without any pretreatment (Table 2). Further, compared with the LHW pretreatment, the optimal LHW-$FeCl_3$ pretreatment significantly increased hexose yields by up to 4–7 times. Although wheat straw was of the highest hexose yield of 93 % (% cellulose) among three bioenergy crops, *Miscanthus* stalk showed much higher total sugar (hexoses + pentoses) yield of 34 % (% dry matter) than those of wheat and *Eucalyptus* at 27 % and 31 % under the optimal LHW-$FeCl_3$ pretreatment conducted, which could be mainly due to relatively high proportions of cellulose and hemicellulose in *Miscanthus* stalk. Therefore, although the three types of bioenergy crops provided distinct lignocellulose substrates, the optimal LHW-$FeCl_3$ pretreatment provided an integrative enhancement of biomass enzymatic saccharification.

Table 1
Lignocellulose composition (% dry matter) of bioenergy crops.

Sample	Cellulose	Hemicellulose	Lignin
Miscanthus	40.91 ± 0.89	26.35 ± 0.34	23.32 ± 0.10
Wheat	26.97 ± 0.25	27.91 ± 0.67	20.98 ± 0.96
Eucalyptus	32.33 ± 0.27	19.53 ± 0.43	25.73 ± 0.73

Data as means ± SD (n = 3).

Table 2
Biomass saccharification of pretreated lignocelluloses in bioenergy.

Sample	Pretreatment	Hexoses yield (% cellulose)	Enzymatic total sugar (% dry matter)
Miscanthus	RAW	6.58 ± 0.34	3.62 ± 0.14
	LHW	12.09 ± 0.27**	7.10 ± 0.14**
	LHW + $FeCl_3$	77.43 ± 1.45**	34.20 ± 0.65**
Wheat	RAW	18.05 ± 1.19	6.86 ± 0.34
	LHW	27.59 ± 1.54**	13.28 ± 0.63**
	LHW + $FeCl_3$	92.68 ± 1.03**	26.93 ± 0.15**
Eucalyptus	RAW	6.81 ± 0.06	2.92 ± 0.04
	LHW	13.58 ± 1.39**	5.74 ± 0.42**
	LHW + $FeCl_3$	87.85 ± 2.34**	30.83 ± 0.80**

Hexose and total sugar yields under optimal LHW at 150 °C for 10 min without/with 4 % $FeCl_3$ Data as means ± SD (n = 3); ** As significant difference between pretreated lignocellulose and raw material (RAW) at $p < 0.01$ level; # Total sugars includes all hexoses and pentoses from enzymatic hydrolysis.

3.2. Upgraded bioethanol production via engineered yeast fermentation in *Miscanthus*

To evaluate the significantly enhanced biomass saccharification due to the optimal LHW-$FeCl_3$ pretreatment, we performed classic ethanol fermentation using two yeast strains (Angel and E4) and enzymatic hydrates from three bioenergy crops (Fig. 2A). Under the optimal LHW-$FeCl_3$ pretreatment, three bioenergy crops could produce the bioethanol yields from 9 % to 13 % (% dry matter), but they only had the bioethanol yields from 2 % to 6 % under LHW pretreatment (Fig. 2B–D; Table S1), which was consistent with the vastly different biomass saccharification examined (Table 2). Because our previously engineered yeast strain (E4) is capable of converting xylose into ethanol [25], this study also resulted in consistently higher bioethanol yields via E4 fermentation compared to the commercial yeast strain (Angel), confirming the effective co-conversion of hexoses and xylose by the E4 strain. We analyzed all hexoses and pentoses that were released from enzymatic hydrolysis in three bioenergy crops. The results indicated that the theoretical total bioethanol yield from *Miscanthus* could reach up to 18 % (% dry matter), considering the co-conversion of all hexoses and pentoses (Fig. 2E). Thus, the results revealed a green strategy for high-yield bioethanol production involving the integration of the optimal LHW-$FeCl_3$ pretreatment with engineered yeast strains in bioenergy crops.

3.3. Dual enhancements of Cd and Cr adsorptions with biosorbents generated from fermentation residues and pretreatment supernatants

As the lignocellulose substrates of the three bioenergy crops could be converted into high-yield bioethanol under the green-like LHW-$FeCl_3$ pretreatment, liquid pretreatment supernatants and solid fermentation residues were produced. To avoid any solid biomass and liquid chemical release, we attempted to generate two biosorbents (termed as FR and FR-PS) by performing mixed-chemical (NaOH and H_2O_2) oxidation reactions with the LHW-$FeCl_3$ pretreatment supernatant (PS) and solid fermentation residue (FR) remaining after bioethanol production (Fig. 3A, Table S2). To explore the functions of two biosorbents, we examined their adsorption capacities with two cationic and anionic

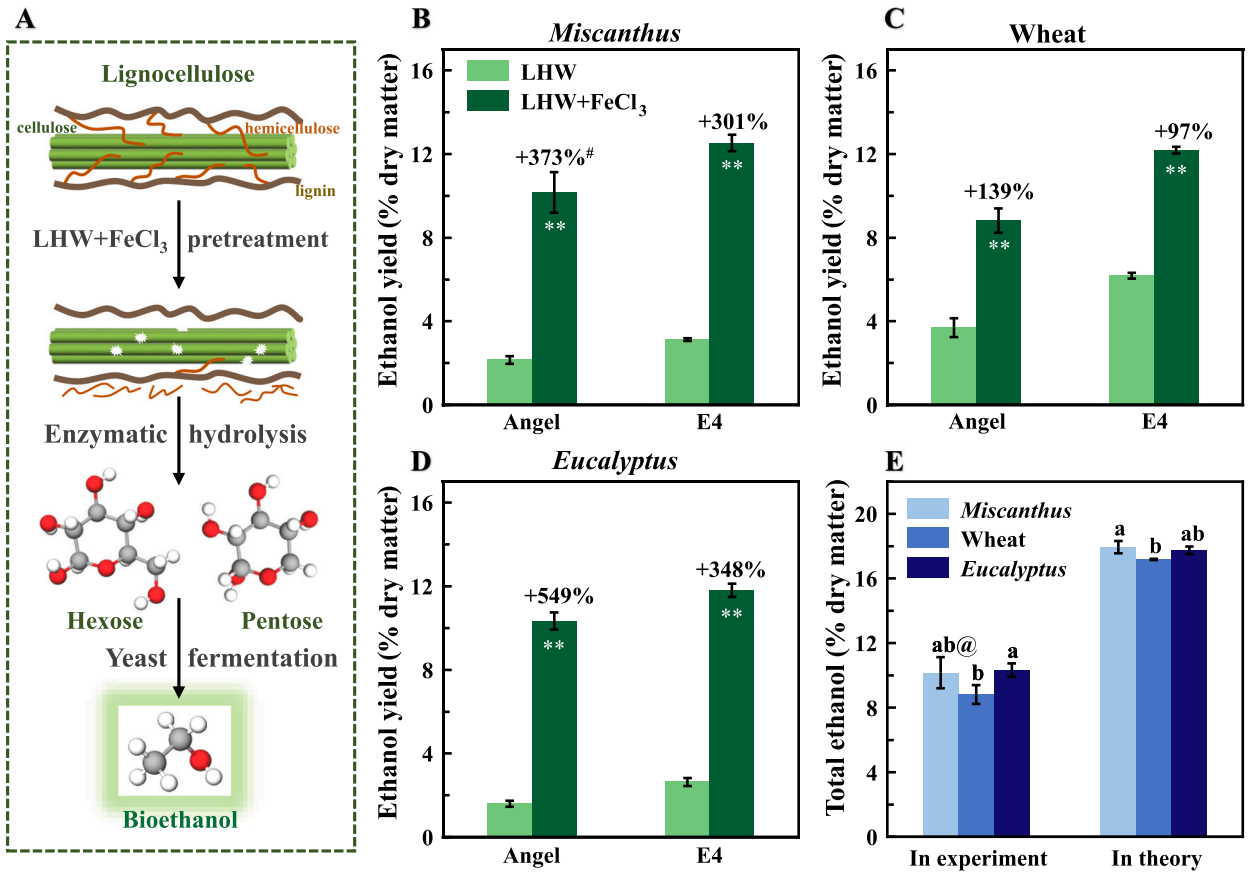

Fig. 2. Bioethanol production from two yeast strains (Angel, E4) fermentations with hexoses released from enzymatic hydrolysis of pretreated lignocelluloses in three major crops (*Miscanthus*, wheat, *Eucalyptus*). (A) Experimental flow chart; (B–D) Comparison of the bioethanol yields by two yeast strains using hexoses and pentoses released from enzymatic hydrolysis under liquid hot water (LHW) and optimal integrated (LHW + $FeCl_3$) pretreatments; (E) Bioethanol yield by yeast (Angel) fermentation in lab-scale experiment using hexoses released from enzymatic hydrolysis after optimal pretreatment and total bioethanol yield by estimating total sugars conversions into ethanol in theory using all hexoses and pentoses released from both optimal pretreatment (LHW + $FeCl_3$) and enzymatic hydrolysis; Data as means ± SD ($n = 3$); @ As multiple significant differences among three bioenergy crops at $p < 0.05$ level by analyses of variance (ANOVA); ** As significant difference between two yeast strains at $p < 0.01$ level; # As increased rate between two pretreatments conducted.

metals (Cd^{2+} and Cr(VI)). Compared with the controls (Raw biosorbents) generated from oxidation reaction with raw biomass, the FR biosorbents of three bioenergy crops showed significantly high Cd^{2+}-adsorption capacities (19.97–25.17 mg/g) at $p < 0.01$ level ($n = 3$), with adsorption increasing by 5.2–8.8 times, whereas the FR-PS biosorbents displayed less increased Cd-adsorption capacities (2.4–3.7 times; Table S2), which should be partially due to Fe^{3+} competition with Cd^{2+} in the FR-PS biosorbents. By contrast, the FR-PS biosorbents showed much higher (2.1–11.7 times) Cr(VI)-adsorption capacities than the raw biomass, whereas the FR biosorbents exhibited less increased Cr(VI)-adsorption capacities (1.4–7.6 times); these result suggest that the PS should provide active chemical groups and Fe^{3+} for enhancing Cr(VI) adsorption in the FR-PS biosorbents. The FR of wheat showed the highest Cd^{2+}-adsorption capacity (25.17 mg/g). The FR-PS of *Eucalyptus* remained the maximum Cr(VI) adsorption at 19.75 mg/g, suggesting that both FR/wheat and FR-PS/*Eucalyptus* should be the desirable biosorbents applicable for two heavy metals adsorptions among all biosorbents of three bioenergy crops examined.

Furthermore, in this study, we incubated different amounts of Cd^{2+} and Cr(VI) into the two desirable biosorbents (Fig. 3B–E). As the initial concentration of Cd^{2+} rose from 10 to 40 mg/L, the FR/wheat biosorbent showed a gradually increasing Cd^{2+}-adsorption capacity (from 9.57 to 25.17 mg/g) and decreasing adsorption efficiency (from 98 % to 65 %; Fig. 3B), which confirmed efficient Cd^{2+} adsorption. Similarly, when the concentration of Cr(VI) increased from 20 to 100 mg/L, the FR-PS/*Eucalyptus* biosorbent exhibited a rising adsorption capacity (from 19.45 to 56.29 mg/g) and a slowly reducing adsorption efficiency (from 99 % to 57 %; Fig. 3C). Notably, the two desirable biosorbents (FR/wheat and FR-PS/*Eucalyptus*) exhibited fast adsorption of the two heavy metals. Their maximum adsorption capacities were reached after 60 min of incubation (Fig. 3D, E). Further isothermal adsorption of the FR/wheat biosorbent showed the R^2 values (0.992 and 0.958) for the Langmuir and Freundlich models, respectively (Table S3), indicating significant chemical interactions with Cd^{2+}. In comparison, the FR-PS/*Eucalyptus* biosorbent had high R^2 values (0.982 and 0.991) for the two models, suggesting that both active physical and chemical interactions should occur for CR(VI) adsorption. Notably, the kinetic parameters of the pseudo-second-order equations revealed extremely high R^2 values (0.9999) for the two biosorbents (Table S4), indicating active chemical adsorption of the two heavy metals. In addition, we compared two desirable biosorbents with previously reported ones generated from other biomass processes (Table 3) [27,28,40–46]. The FR/wheat and FR-PS/*Eucalyptus* samples exhibited the highest Cd^{2+}- and Cr(VI)-adsorption capacities among all comparable biosorbents, reconfirming that the two desirable biosorbents should be optimal for the removal of the two heavy metals.

3.4. Characterization of desirable wheat and Eucalyptus biosorbents for maximizing Cd^{2+} and Cr(VI) adsorptions

To understand FR/wheat and FR-PS/*Eucalyptus* defined as desirable biosorbents for Cd^{2+}/Cr(VI) adsorption, we conducted a typical X-ray

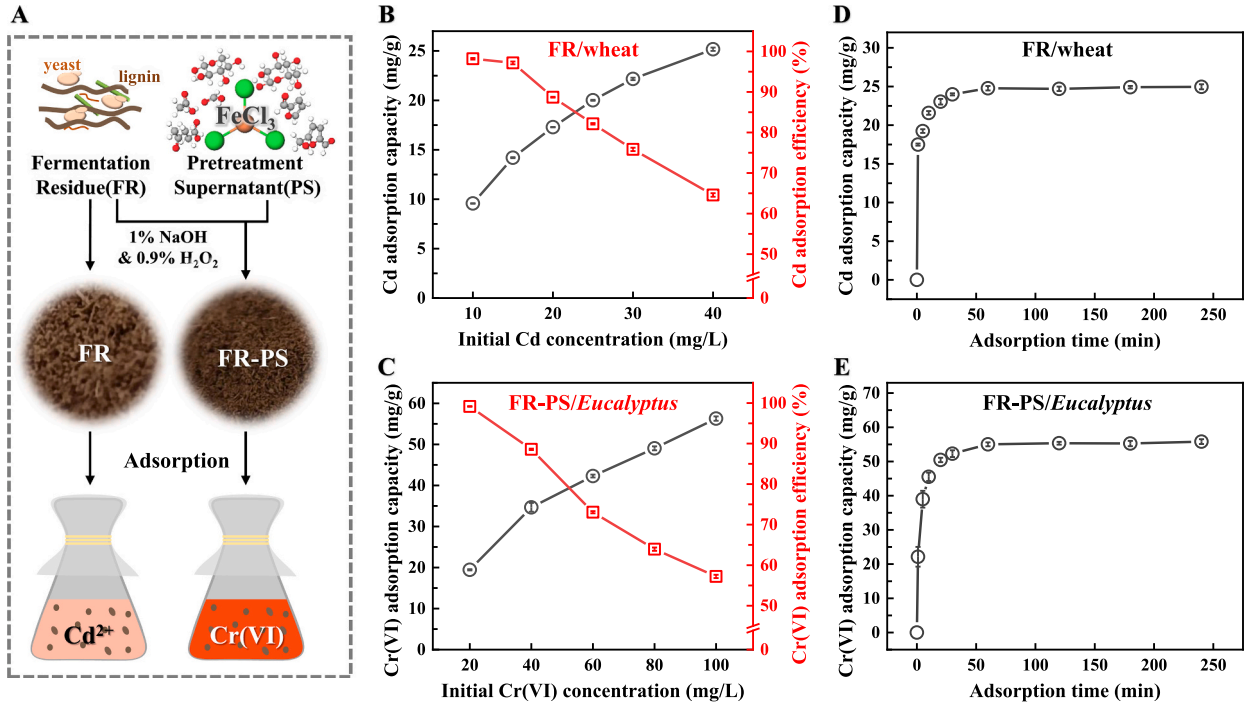

Fig. 3. Distinct heavy metal adsorption capacities of two biosorbents generated by oxidation reaction with fermentation residues (FR) and optimal (LHW + $FeCl_3$) pretreatment supernatant (PS). (A) Experimental flow chart; (B, D) Cd adsorption capacity and efficiency with FR biosorbent of wheat; (C, E) Cr(VI) adsorption capacity and efficiency FR-PS biosorbent of *Eucalyptus*.

photoelectron spectroscopy (XPS) assay for the chemical properties of biosorbents (Fig. 4). Compared with the controls without heavy-metal incubation, the two biosorbents (FR/wheat and FR-PS/*Eucalyptus*) exhibited typical peaks for Cd^{2+} and Cr(VI) adsorptions on the XPS profile, and the proportions of characteristic peaks attributed to carbon and oxygen elements (C1s and O1s) were relatively altered after Cd^{2+} and Cr(VI) adsorption (Fig. 4A, B), providing direct evidence of the formation of new chemical bonds between metals and biosorbents. The Cd 3d spectrum was divided into two peaks ($3d^3$, Cd—O) corresponding to 412.64 and 405.82 eV. In contrast, the Cr 2p spectrum was split into three peaks on the $2p^1$ and $2p^3$ orbitals corresponding to the metallic and oxidized states of Cr (Fig. S2A, B). Moreover, three peaks (O=C–O, C—O, and C–C/C–H) were identified for C 1s, but only the O=C–O peak was altered because of Cd^{2+} adsorption (Figs. 4C; S2C). As the O1s peak was not changed owing to Cd^{2+} interaction with the biosorbent (Figs. 4E; S2E), we assumed that the adsorption of Cd ions by FR/wheat was mainly due to Cd–-O formation via the O=C–O group [47]. Similarly, only the C—O peak was altered in the FR-PS/*Eucalyptus* biosorbent from Cr(VI) adsorption (Figs. 4D, F; S2D, F), which also indicated that the oxygen-containing functional group was mainly involved in the interaction of Cr(VI) with the biosorbent.

Furthermore, two biosorbents (FR/wheat and FR-PS/*Eucalyptus*) surfaces were observed under scanning electron microscopy (SEM; Fig. 5A, B). Even though both biosorbents were typically porous structures accounting for the high porosity for metal adsorption, FR-PS/*Eucalyptus* exhibited evener and rougher surfaces, which could be due to the accumulation of diverse organic carbons in the LHW-$FeCl_3$ pretreatment. Under Fourier transform infrared scanning, the two biosorbents showed several altered peaks relative to their raw materials (Fig. 5C, D; Table S5), confirming partial hemicellulose and lignin co-extraction from the optimal LHW-$FeCl_3$ pretreatments. Few altered peaks existed between the FR and FR-PS samples of wheat and *Eucalyptus*, suggesting that Fe^{3+} and organic carbon may not be chemically interlinked with FR. This also explains why free Fe^{3+} competes with Cd^{2+}, leading to less Cd adsorption in FR-PS relative to FR. Thus, we confirmed that the two biosorbents (FR/wheat and FR-PS/*Eucalyptus*) have raised surfaces and porosity enables multiple active and functional group interactions with the two heavy metals examined.

3.5. Desired biochar generation from Miscanthus enzyme-undigestible residue for dye adsorption

As biomass enzymatic saccharification is an essential step for almost all renewable biofuels and valuable bioproducts [14], enzymatically indigestible residues in bioenergy crops should be recycled. Using the enzyme-undigestible residues of the three bioenergy crops, we performed KOH-activated thermal-chemical conversions to generate biochar samples (Fig. 6A). To test the functions of all biochar samples, we examined their adsorption capacities with two cationic and anionic dyes (MB and CR). The *Miscanthus* sample showed relatively higher dye adsorption capacities than the wheat and *Eucalyptus* samples (Table S6). This study also generated biochar samples using the raw biomass materials of the three bioenergy crops. The *Miscanthus* sample consistently showed higher dye adsorption (Table S6), indicating that *Miscanthus* could provide the desired lignocellulose structure for high-performance biochar assembly. Notably, the three biochar samples of enzyme-undigestible residues had significantly higher dye adsorption capacities than their raw materials ($p < 0.01$ level ($n = 3$)), particularly for MB adsorption.

In terms of the *Miscanthus* biochar sample with the highest adsorption capacity, we further examined its adsorption of different concentrations of dyes under a time course of incubation (Fig. 6B–E). The *Miscanthus* biochar showed a fast dye-adsorption, reaching the maximum capacity within 60 min, and it also displayed high adsorption efficiencies of 100 % (CR) and 97 % (MB). Isotherm modeling revealed high R^2 values for the Langmuir (0.994 and 0.998 for MB) and Freundlich models (0.981 and 0.988 for CR) (Table S7), indicating major chemical interactions between the biochar and dye. Furthermore, the pseudo-second-order equations indicated extremely high R^2 values (0.9999) for MB and CR adsorption (Table S8), which confirmed that the

Table 3
Comparison of Cd^{2+} and Cr (VI) adsorption capacities with the biosorbents generated in this study and from previously-reported ones.

Biosorbent	Method	Maximum adsorption (mg/g)	Reference
	Dried fermentation residues	Cd^{2+}	
Wheat/FR	immersed in 1 % NaOH with 0.9 % H_2O_2 at 50 °C	25.17	This study
Areca waste	Added in 0.2 M NaOH for 12 h, immersed into 0.2 M H_2SO_4 for 12 h, and dried at 105 °C	1.12	(Zheng et al. 2008)
Coconut copra meal	Sun dried, crushed to 250 μm, and soaked in 0.02 M HCl overnight	4.99	(Ho et al. 2006)
Green coconut	Added 0.1 M NaOH 3 h, washed with deionized water, and dried at 50 °C	11.96	(Sousa et al. 2010)
Raw rice husk	Selected particle between 425 and 600 μm, washed with distilled water and dried at 60 °C	8.58	(Kumar et al. 2006)
Spent coffee grounds	Air dried for two weeks, passed through a 0.5-mm sieve, and without any pretreatment	19.32	(Kim et al. 2020)
	Dried fermentation residues	Cr(VI)	
Eucalyptus/ FR-PS	with $FeCl_3$ pretreatment supernatants, immersed in 1 % NaOH with 0.9 % H_2O_2 at 50 °C	19.75	This study
Banana peel	Dried at 60 °C for 24 h, crushed to 125 μm, washing with pure water and 0.1 M HCl	10.4	(Parlayici et al. 2019)
Cranberry kernel shell	Dried at 60 °C for 24 h, crushed to 125 μm, washing with pure water and 0.1 M HCl	6.8	(Parlayici et al. 2019)
Groundnut husk	Added sulfuric acid in 4:3 ratio, 150–155 °C for 24 h, and impregnated 1 % silver nitrate	11.4	(Dubey et al. 2007)
Sugarcane bagasse	Dried at 110 °C for 24 h, and sieved through a BS Sieve No. 14	13.4	(Sharma et al. 1994)
Tea (*Camellia sinesis*)	Crushed to 255-mesh, Added 0.1 N NaOH for 9 h, and dipped into 0.1 N H_2SO_4 for 9 h	7.3	(Islam et al. 2019)

biochar generated from the enzyme-undigestible residue of *Miscanthus* could be more effective for dye adsorption via active chemical interactions.

3.6. Characterization of Miscanthus biochar having high porosity and graphene-like structure

With respect to the desirable biochar generated from the enzyme-undigestible residue of *Miscanthus* straw, we observed the surface morphology of the biosorbent under SEM and exhibited a tide-like assembly with a three-dimensional porous structure (Fig. 7A). To understand such a highly porous carbon assembly, we measured the biochar porosity by performing a classic Brunauer–Emmett–Teller assay (Fig. 7B, C). In comparison, the desirable biochar (residue) had a much larger surface area (2967 m^2/g) and total pore volume (1.73 cm^2/g) than those of the control (Raw) generated from raw biomass material of *Miscanthus* straw, with increased surface area and pore volume of 88 % and 67 %, respectively. Such upgraded carbon porosity should account for the significantly increased dye-adsorption capacity observed with the desirable biochar (Fig. 6). X-ray diffraction revealed that the Raw biochar exhibited a series of peaks, including the diffraction peaks of (002) and (100) crystal planes of graphite at 2θ angles of 24.9° and 43.6°, respectively. In contrast, the Residue biochar displayed weak peaks at 2θ angles of 24° and 44° (Fig. 7D), suggesting that the ordered graphite carbon layers should be more damaged in the Residue biochar sample. To confirm this finding, Raman scanning was conducted to observe three prominent characteristic peaks (D, G, and 2D) accounting for the carbon graphite properties (Fig. 7E). As a result, the residual biochar showed a higher I_D/I_G ratio than that of the Raw biochar sample, revealing a relatively higher degree of defects in the desired biochar [48,49]. As the two biochar samples did not show a 2D peak, which should appear between 2260 and 2700 cm^{-1} of Raman spectra accountable for graphene-like nanocarbon [50], they should not contain any graphene carbon, which may be helpful for active chemical interactions between the biochar and the organic dyes examined.

3.7. Mechanistic model representing optimal lignocellulose conversions and recycling for high-yield bioethanol and high-efficiency bio-adsorption

By integrating all the major results of this study with those of previous studies, we propose a mechanistic model to explain how three distinct lignocelluloses are optimally selective and completely recyclable for achieving high-yield bioethanol conversion and high-performance biosorbent/biochar assemblies from major agricultural–forestry bioenergy crops (Fig. 8). Owing to their rich lignocellulose deposition, *Miscanthus* straws could provide much more hexoses and pentoses than the other two crop samples through the enzymatic hydrolysis of both cellulose and hemicellulose and lead to a higher total bioethanol yield because of the optimal LHW-$FeCl_3$ pretreatment and engineered yeast strain. Even though efficient biomass enzymatic saccharification was achieved from the optimal green-like pretreatment, the *Miscanthus* sample retained relatively more highly crystalline cellulose nanofibers and a higher proportion of lignin residues than the other two crop samples did; this retention should be favorable when obtaining high-porosity biochar assemblies through active physical and chemical interactions between *Miscanthus* biochars and two characteristic organic dyes (CR and MB). The remaining yeast-fermentation residues in the three bioenergy crops were recycled as functional biosorbents through one-step oxidative reactions. The wheat biosorbent exhibited the highest Cd-adsorption capacity among all biosorbents examined from other previously reported biomass resources; this may mainly be owing to the remaining few cellulose nanofibers and a high proportion of lignin that enabled more chemical groups to be generated for active chemical interaction with Cd. As the optimal LHW-$FeCl_3$ pretreatment is a typical green-like process, we also found the advantage of recycling the pretreatment liquid waste for biosorbent generation. The *Eucalyptus* biosorbent had the highest Cr(VI)-adsorption capacity compared with previously generated biosorbents from other biomass resources. In terms of such findings, the proposed mechanistic model revealed two primary causes: the *Eucalyptus* residue containing high proportions of lignin and yeast cells resulting in high-porosity biosorbent assemblies and the pretreatment supernatant providing free Fe^{3+} and rich organic carbons for effective physical and chemical interactions with Cr(VI). Although this model is aimed at clarifying the mechanism underlying the optimal biomass conversion and green recycling of various lignocellulosic materials obtained from three major agricultural and forestry plants, its applications in other bioenergy crops and the optimization of processing technologies should be explored in the future.

4. Conclusion

By employing distinct lignocelluloses of three representative agriculture/forestry plant species, we performed optimal green-like LHW-$FeCl_3$ pretreatments to enhance enzymatic saccharification and bioethanol yield from engineered-yeast-strain fermentation. The three remaining sources, namely, a high-porosity biochar produced from *Miscanthus* enzyme-undigestible lignocellulose and two high-performance biosorbents generated from wheat and *Eucalyptus* fermentation residues mixed with LHW-$FeCl_3$ pretreatment supernatants, of solid biomass residues and liquid chemical wastes were

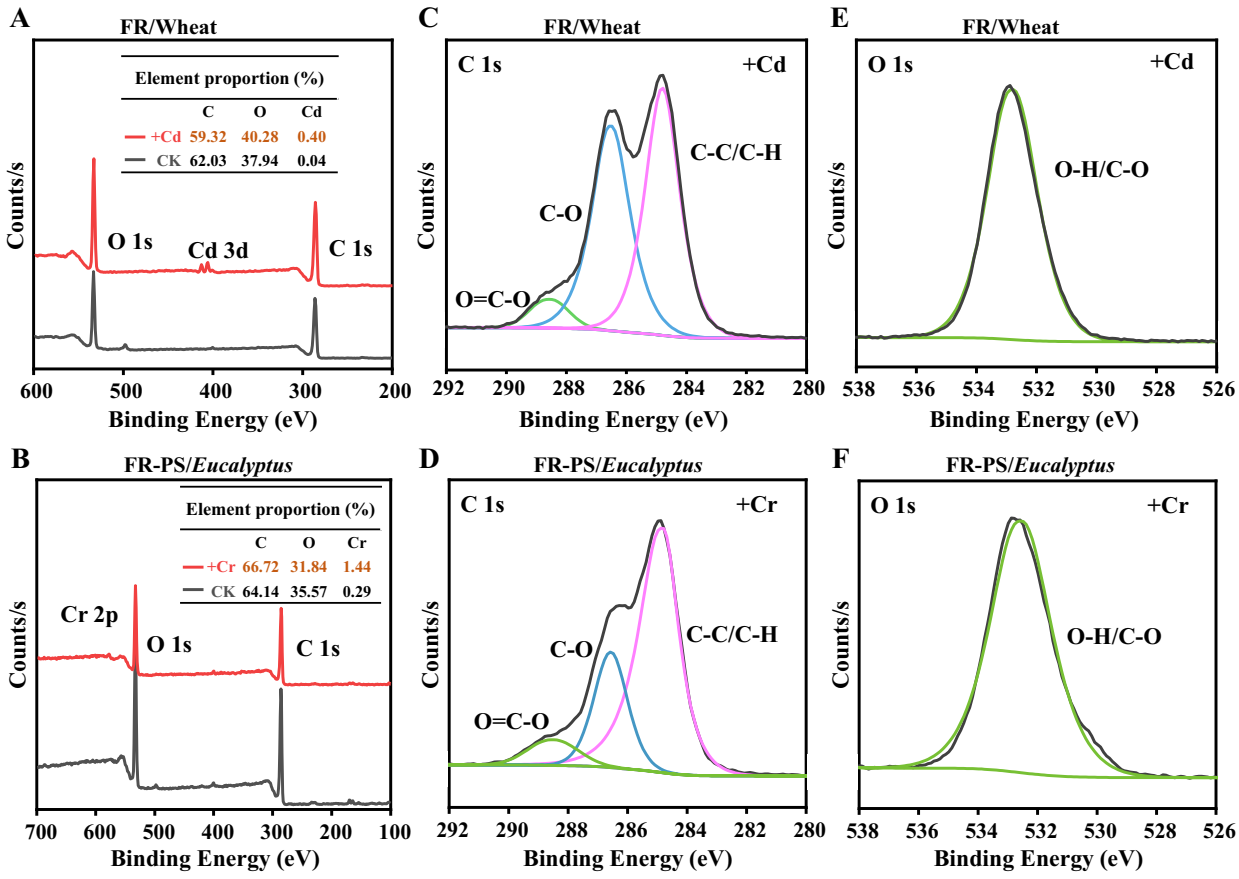

Fig. 4. XPS analysis of Cd^{2+} and Cr (VI) adsorption with two biosorbents (FR/Wheat, FR-PS/*Eucalyptus*). (A, B) XPS spectrum for major elements; (C, D) C 1s spectrum; (E, F) O 1s spectrum.

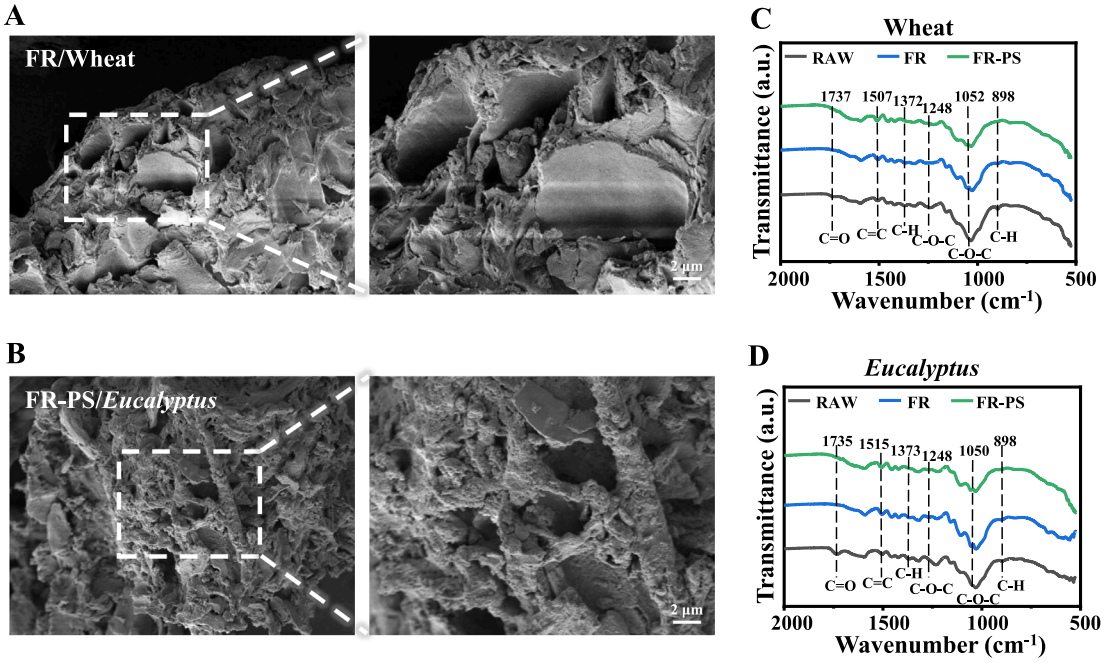

Fig. 5. Characterization of two biosorbents generated from FR/Wheat and FR-PS/ *Eucalyptus.* (A, B) SEM images; (C, D) FTIR spectrum of biosorbents with chemical groups annotated in.

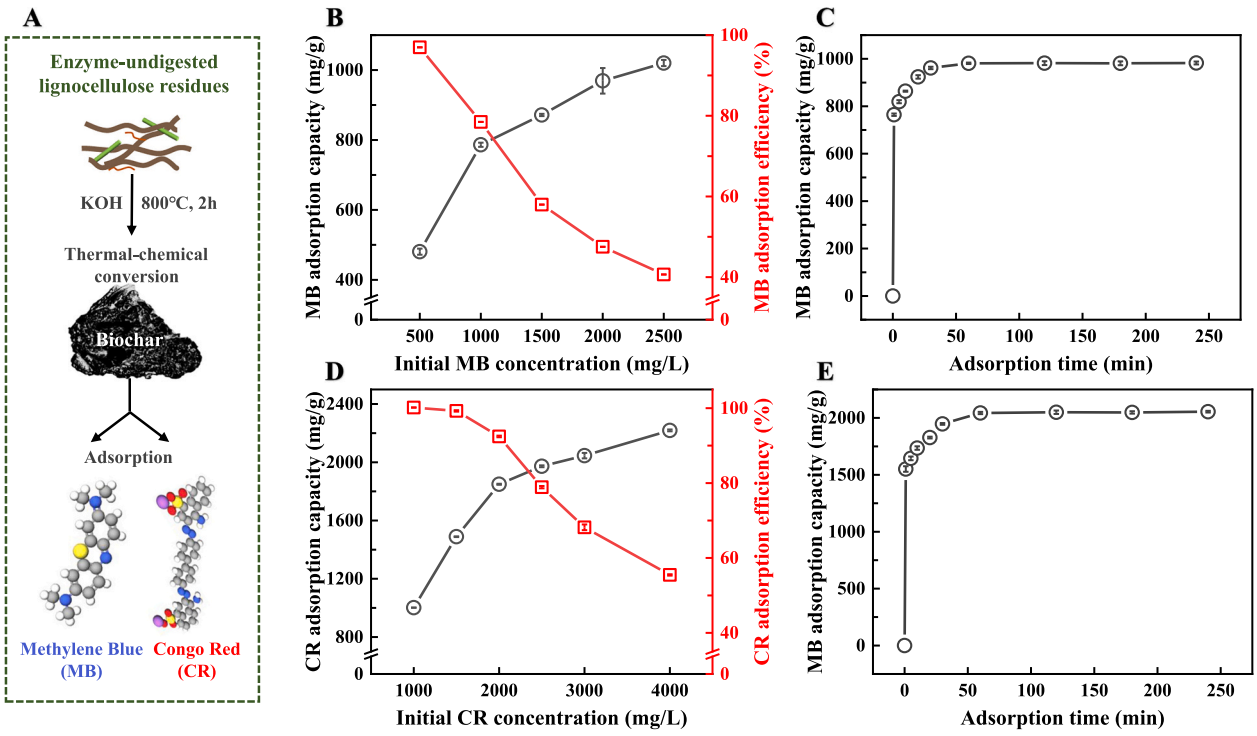

Fig. 6. Analysis of two dyes (MB, CR) adsorptions with the biochar sample generated from enzyme-undigested residue of *Miscanthus* straw after optimal (LHW + $FeCl_3$) pretreatment. (A) Experimental flow chart; (B, D) MB and CR adsorption capacity and efficiency under different initial concentrations of MB and CR at 25 °C with biochar (1.0 g/L) for 4 h; (C, E) Biochar adsorption capacity with MB (initial concentration at 2000 mg/L) and CR (initial concentration at 3000 mg/L) under different incubation time.

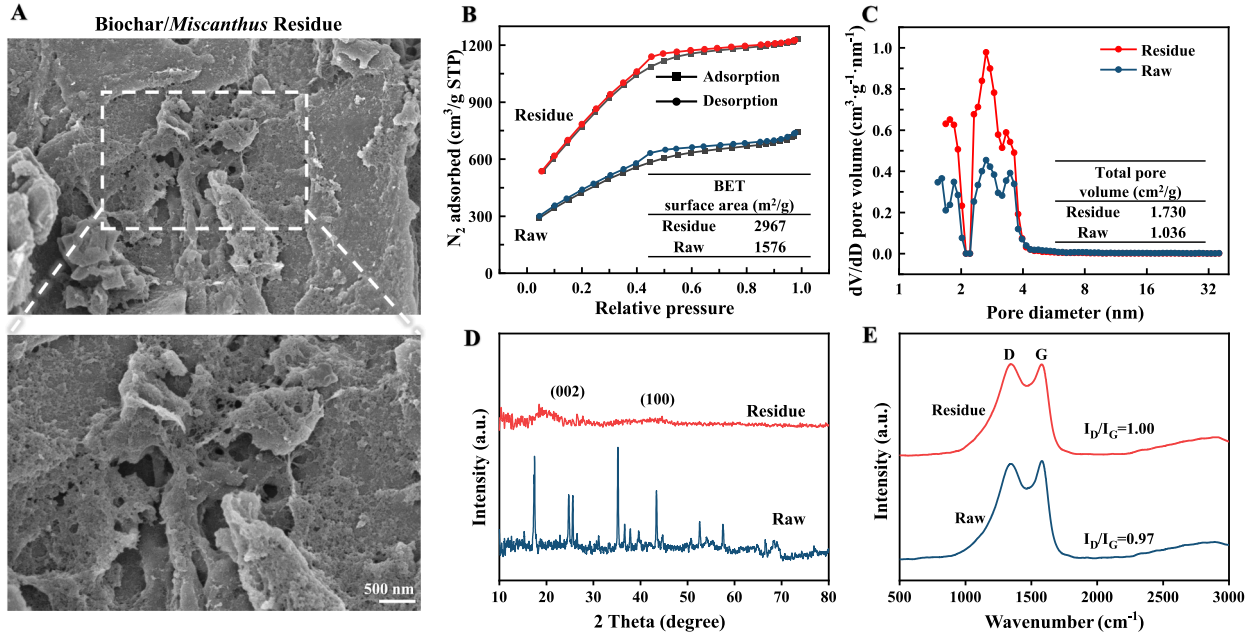

Fig. 7. Characterization of biochar generated from the enzyme-undigested residue of *Miscanthus* straw after optimal (LHW + $FeCl_3$) pretreatment. (A) SEM image of biochar; (B, C) BET analysis of biochar porosity; (D) X-ray assay; (E) Raman-spectra profiling. Raw as biochar generated from raw biomass material of *Miscanthus* straw.

recycled as valuable bioproducts. We not only detected much-upgraded dye adsorption with the desirable biochar but also identified two optimal biosorbents having the highest Cd^{2+}- and Cr(VI)-adsorption capacities. Finally, we developed a mechanistic model to elucidate how distinct lignocelluloses are optimally convertible and recyclable for increasing bioethanol production and maximizing the capacity to bioadsorb heavy metals and organic dyes. Thus, we provided a novel strategy for the fully effective utilization of agricultural–forestry lignocellulose resources under green-like recycling.

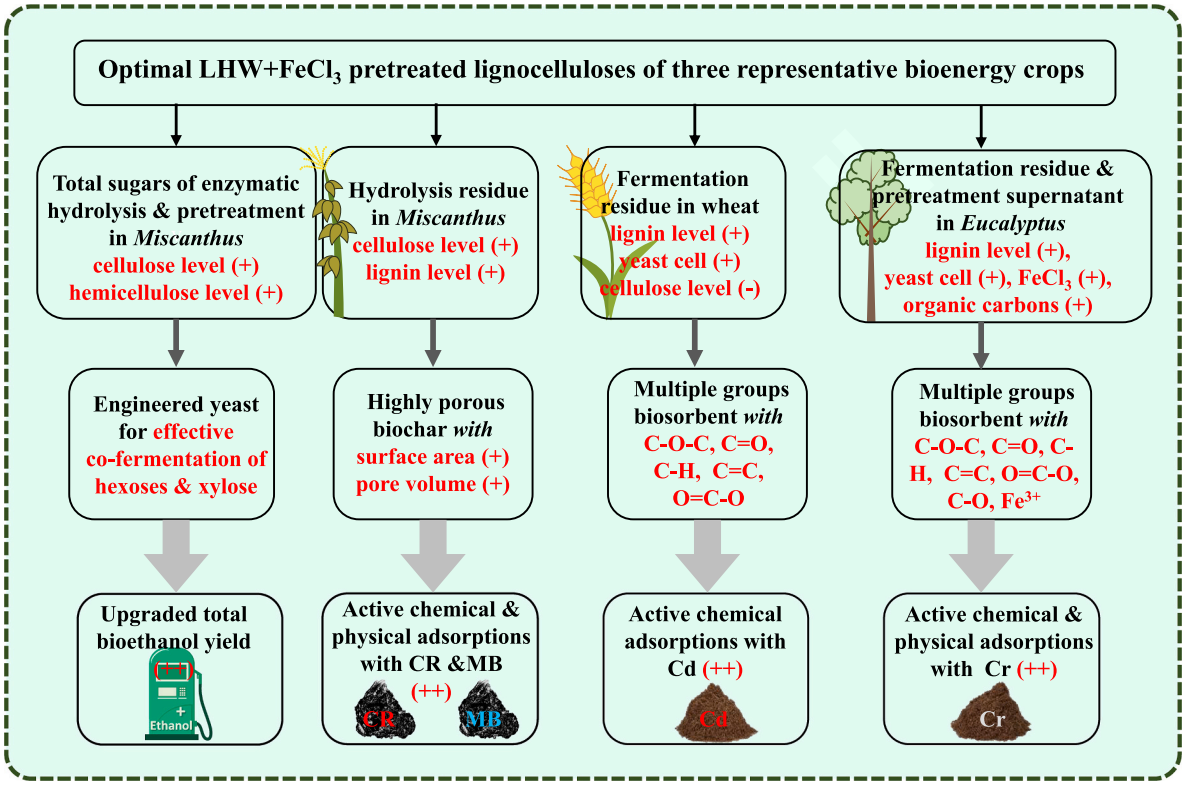

Fig. 8. A mechanism model to elucidate how distinct lignocelluloses of three representative plant species selective for high-yield bioethanol production, two desirable biosorbents assembly for maximizing two heavy metals (Cd, Cr) removals and highly porous biochar generation for two industry dyes (CR, MB) adsorption. (+) & (−) Highlighted as raised & reduced major factor/factor of lignocellulose and biosorbent/biochar.

CRediT authorship contribution statement

Wenbo Yang: Writing – original draft, Methodology, Investigation, Formal analysis. **Boyang He:** Methodology, Investigation, Formal analysis. **Hua Yu:** Methodology, Formal analysis. **Huiyi Zhang:** Methodology, Formal analysis. **Yunong Li:** Methodology, Formal analysis. **Jingyuan Liu:** Methodology, Formal analysis. **Hao Peng:** Methodology, Formal analysis. **Hailang Wang:** Validation, Methodology, Investigation. **Peng Liu:** Writing – review & editing, Validation. **Yanting Wang:** Validation, Methodology, Investigation. **Liangcai Peng:** Writing – review & editing, Validation, Funding acquisition. **Dan Sun:** Writing – review & editing, Supervision, Conceptualization.

Declaration of competing interest

The authors declare that they have no known competing financial interests or personal relationships that could have appeared to influence the work reported in this paper.

Acknowledgments

This work was in part supported by the National Natural Science Foundation of China (32470273, 32170268, 32101701) and the Initiative Grant of Hubei University of Technology for High-level Talents (GCC20230001).

Appendix A. Supplementary data

Supplementary data to this article can be found online at https://doi.org/10.1016/j.ijbiomac.2025.146214.

Data availability

Data will be made available on request.

References

[1] V. Ashokkumar, R. Venkatkarthick, S. Jayashree, S. Chuetor, S. Dharmaraj, G. Kumar, W.H. Chen, C. Ngamcharussrivichai, Recent advances in lignocellulosic biomass for biofuels and value-added bioproducts - a critical review, Bioresour. Technol. 344 (2022) 126195, https://doi.org/10.1016/j.biortech.2021.126195.
[2] R. Zhang, Z. Hu, H. Peng, P. Liu, Y. Wang, J. Li, J. Lu, Y. Wang, T. Xia, L. Peng, High density cellulose nanofibril assembly leads to upgraded enzymatic and chemical catalysis of fermentable sugars, cellulose nanocrystals and cellulase production by precisely engineering cellulose synthase complexes, Green Chem. 25 (3) (2023) 1096–1106, https://doi.org/10.1039/D2GC03744K.
[3] Y. Ai, H. Wang, P. Liu, H. Yu, M. Sun, R. Zhang, J. Tang, Y. Wang, S. Feng, L. Peng, Insights into contrastive cellulose nanofibrils assembly and nanocrystals catalysis from dual regulations of plant cell walls, Sci. Bull. (2024), https://doi.org/10.1016/j.scib.2024.06.013.
[4] H. Hu, R. Zhang, Z. Tao, X. Li, Y. Li, J. Huang, X. Li, X. Han, S. Feng, G. Zhang, L. Peng, Cellulose synthase mutants distinctively affect cell growth and cell wall integrity for plant biomass production in *Arabidopsis*, Plant Cell Physiol. 59 (6) (2018) 1144–1157, https://doi.org/10.1093/pcp/pcy050.
[5] R. Zhang, Z. Hu, Y. Wang, H. Hu, F. Li, M. Li, A. Ragauskas, T. Xia, H. Han, J. Tang, H. Yu, B. Xu, L. Peng, Single-molecular insights into the breakpoint of cellulose nanofibers assembly during saccharification, Nat. Commun. 14 (1) (2023) 1100, https://doi.org/10.1038/s41467-023-36856-8.
[6] Y. Deng, G. Yang, Z. Xie, J. Yu, D. Jiang, Z. Huang, Effects of different weeding methods on the biomass of vegetation and soil evaporation in *Eucalyptus* plantations, Sustainability 12 (9) (2020) 3669, https://doi.org/10.3390/su12093669.
[7] A. Hamid, A. Zafar, S. Latif, L. Peng, Y. Wang, I. Liaqat, M.S. Afzal, M.N. Aftab, Enzymatic hydrolysis of low temperature alkali pretreated wheat straw using immobilized β-xylanase nanoparticles, RSC Adv. 13 (2) (2023) 1434–1445.
[8] G. Xie, L. Peng, Genetic engineering of energy crops: a strategy for biofuel production in China, J. Integr. Plant Biol. 53 (2) (2011) 143–150, https://doi.org/10.1111/j.1744-7909.2010.01022.x.
[9] L. Cheng, L. Wang, L. Wei, Y. Wu, A. Alam, C. Xu, Y. Wang, Y. Tu, L. Peng, T. Xia, Combined mild chemical pretreatments for complete cadmium release and cellulosic ethanol co-production distinctive in wheat mutant straw, Green Chem. 21 (13) (2019) 3693–3700, https://doi.org/10.1039/C9GC00686A.

[10] R. Kumar, T.H. Kim, B. Basak, S.M. Patil, H.H. Kim, Y. Ahn, K.K. Yadav, M.M. S. Cabral-Pinto, B.H. Jeon, Emerging approaches in lignocellulosic biomass pretreatment and anaerobic bioprocesses for sustainable biofuels production, J. Clean. Prod. 333 (2022) 130180, https://doi.org/10.1016/j.jclepro.2021.130180.
[11] M. Wang, Y. Wang, J. Liu, H. Yu, P. Liu, Y. Yang, D. Sun, H. Kang, Y. Wang, J. Tang, C. Fu, L. Peng, Integration of advanced biotechnology for green carbon, Green Carbon 2 (2) (2024) 164–175, https://doi.org/10.1016/j.greenca.2024.02.006.
[12] Z. Li, C. Zhao, Y. Zha, C. Wan, S. Si, F. Liu, R. Zhang, F. Li, B. Yu, Z. Yi, N. Xu, L. Peng, Q. Li, The minor wall-networks between monolignols and interlinked-phenolics predominantly affect biomass enzymatic digestibility in *Miscanthus*, PloS One 9 (8) (2014) e105115, https://doi.org/10.1371/journal.pone.0105115.
[13] L. Wu, M. Li, J. Huang, H. Zhang, W. Zou, S. Hu, Y. Li, C. Fan, R. Zhang, H. Jing, L. Peng, S. Feng, A near infrared spectroscopic assay for stalk soluble sugars, bagasse enzymatic saccharification and wall polymers in sweet sorghum, Bioresour. Technol. 177 (2015) 118–124, https://doi.org/10.1016/j.biortech.2014.11.073.
[14] R. Zhang, H. Gao, Y. Wang, B. He, J. Lu, W. Zhu, L. Peng, Y. Wang, Challenges and perspectives of green-like lignocellulose pretreatments selectable for low-cost biofuels and high-value bioproduction, Bioresour. Technol. 369 (2023) 128315, https://doi.org/10.1016/j.biortech.2022.128315.
[15] Y. Wang, J. Huang, Y. Li, K. Xiong, Y. Wang, F. Li, M. Liu, Z. Wu, Y. Tu, L. Peng, Ammonium oxalate-extractable uronic acids positively affect biomass enzymatic digestibility by reducing lignocellulose crystallinity in *Miscanthus*, Bioresour. Technol. 196 (2015) 391–398, https://doi.org/10.1016/j.biortech.2015.07.099.
[16] M. Hu, H. Yu, Y. Li, A. Li, Q. Cai, P. Liu, Y. Tu, Y. Wang, R. Hu, B. Hao, L. Peng, T. Xia, Distinct polymer extraction and cellulose DP reduction for complete cellulose hydrolysis under mild chemical pretreatments in sugarcane, Carbohydr. Polym. 202 (2018) 434–443, https://doi.org/10.1016/j.carbpol.2018.08.039.
[17] J.M. Wells, E. Drielak, K.C. Surendra, S. Kumar Khanal, Hot water pretreatment of lignocellulosic biomass: modeling the effects of temperature, enzyme and biomass loadings on sugar yield, Bioresour. Technol. 300 (2020) 122593, https://doi.org/10.1016/j.biortech.2019.122593.
[18] W.H. Chen, S. Nižetić, R. Sirohi, Z. Huang, R. Luque, A.M. Papadopoulos, R. Sakthivel, X. Phuong Nguyen, A. Tuan Hoang, Liquid hot water as sustainable biomass pretreatment technique for bioenergy production: a review, Bioresour. Technol. 344 (2022) 126207, https://doi.org/10.1016/j.biortech.2021.126207.
[19] J. Li, F. Liu, H. Yu, Y. Li, S. Zhou, Y. Ai, X. Zhou, Y. Wang, L. Wang, L. Peng, Y. Wang, Diverse banana pseudostems and rachis are distinctive for edible carbohydrates and lignocellulose saccharification towards high bioethanol production under chemical and liquid hot water pretreatments, Molecules 26 (13) (2021) 3870, https://doi.org/10.3390/molecules26133870.
[20] S.R. Kamireddy, J. Li, M. Tucker, J. Degenstein, Y. Ji, Effects and mechanism of metal chloride salts on pretreatment and enzymatic digestibility of corn Stover, Ind. Eng. Chem. Res. 52 (5) (2013) 1775–1782, https://doi.org/10.1021/ie3019609.
[21] J. Liu, X. Zhang, H. Peng, T. Li, P. Liu, H. Gao, Y. Wang, J. Tang, Q. Li, Z. Qi, L. Peng, T. Xia, Full-chain $FeCl_3$ catalyzation is sufficient to boost cellulase secretion and cellulosic ethanol along with valorized supercapacitor and biosorbent using desirable corn stalk, Molecules 28 (5) (2023) 2060, https://doi.org/10.3390/molecules28052060.
[22] J.M. Bracher, O.A. Martinez-Rodriguez, W.J.C. Dekker, M.D. Verhoeven, A.J.A. van Maris, J.T. Pronk, Reassessment of requirements for anaerobic xylose fermentation by engineered, non-evolved *Saccharomyces cerevisiae* strains, FEMS Yeast Res. 19 (1) (2019) foy104, https://doi.org/10.1093/femsyr/foy104.
[23] M. Madadi, K. Zhao, Y. Wang, Y. Wang, S.w. Tang, T. Xia, N. Jin, Z. Xu, G. Li, Z. Qi, L. Peng, Z. Xiong, Modified lignocellulose and rich starch for complete saccharification to maximize bioethanol in distinct polyploidy potato straw, Carbohydr. Polym. 265 (2021) 118070, https://doi.org/10.1016/j.carbpol.2021.118070.
[24] A. Ochoa-Chacón, A. Martinez, H.M. Poggi-Varaldo, L. Villa-Tanaca, A.C. Ramos-Valdivia, T. Ponce-Noyola, Xylose metabolism in bioethanol production: *Saccharomyces cerevisiae* vs non-*Saccharomyces* yeasts, Bioenergy Res. 15 (2) (2022) 905–923, https://doi.org/10.1007/s12155-021-10340-x.
[25] B. He, B. Hao, H. Yu, F. Tu, X. Wei, K. Xiong, Y. Zeng, H. Zeng, P. Liu, Y. Tu, Y. Wang, H. Kang, L. Peng, T. Xia, Double integrating *XYL2* into engineered *Saccharomyces cerevisiae* strains for consistently enhanced bioethanol production by effective xylose and hexose co-consumption of steam-exploded lignocellulose in bioenergy crops, Renew. Energ. 186 (2022) 341–349, https://doi.org/10.1016/j.renene.2021.12.103.
[26] H. Yu, M. Hu, Z. Hu, F. Liu, H. Yu, Q. Yang, H. Gao, C. Xu, M. Wang, G. Zhang, Y. Wang, T. Xia, L. Peng, Y. Wang, Insights into pectin dominated enhancements for elimination of toxic Cd and dye coupled with ethanol production in desirable lignocelluloses, Carbohydr. Polym. 286 (2022) 119298, https://doi.org/10.1016/j.carbpol.2022.119298.
[27] Ş. Parlayici, E. Pehlivan, Comparative study of Cr(VI) removal by bio-waste adsorbents: equilibrium, kinetics, and thermodynamic, J. Anal. Sci. Technol. 10 (1) (2019) 15, https://doi.org/10.1186/s40543-019-0175-3.
[28] Y.S. Ho, A.E. Ofomaja, Biosorption thermodynamics of cadmium on coconut copra meal as biosorbent, Biochem. Eng. J. 30 (2) (2006) 117–123, https://doi.org/10.1016/j.bej.2006.02.012.
[29] Z. Hu, Q. Li, Y. Chen, T. Li, Y. Wang, R. Zhang, H. Peng, H. Wang, Y. Wang, J. Tang, M. Nauman Aftab, L. Peng, Intermittent ultrasound retains cellulases unlock for enhanced cellulosic ethanol with high-porosity biochar for dye adsorption using desirable rice mutant straw, Bioresour. Technol. 369 (2023) 128437, https://doi.org/10.1016/j.biortech.2022.128437.
[30] L. Peng, C.H. Hocart, J.W. Redmond, R.E. Williamson, Fractionation of carbohydrates in *Arabidopsis* root cell walls shows that three radial swelling loci are specifically involved in cellulose production, Planta 211 (3) (2000) 406–414, https://doi.org/10.1007/s004250000301.
[31] J. Jia, B. Yu, L. Wu, H. Wang, Z. Wu, M. Li, P. Huang, S. Feng, P. Chen, Y. Zheng, L. Peng, Biomass enzymatic saccharification is determined by the non-KOH-extractable wall polymer features that predominately affect cellulose crystallinity in corn, PloS One 9 (9) (2014) e108449, https://doi.org/10.1371/journal.pone.0108449.
[32] W. Jin, L. Chen, M. Hu, D. Sun, A. Li, Y. Li, Z. Hu, S. Zhou, Y. Tu, T. Xia, Y. Wang, G. Xie, Y. Li, B. Bai, L. Peng, Tween-80 is effective for enhancing steam-exploded biomass enzymatic saccharification and ethanol production by specifically lessening cellulase absorption with lignin in common reed, Appl. Energ. 175 (2016) 82–90, https://doi.org/10.1016/j.apenergy.2016.04.104.
[33] L. Wu, S. Feng, J. Deng, B. Yu, Y. Wang, B. He, H. Peng, Q. Li, R. Hu, L. Peng, Altered carbon assimilation and cellulose accessibility to maximize bioethanol yield under low-cost biomass processing in corn brittle stalk, Green Chem. 21 (16) (2019) 4388–4399, https://doi.org/10.1039/C9GC01237K.
[34] P. Liu, Y. Wang, H. Kang, Y. Wang, H. Yu, H. Peng, B. He, C. Xu, K.Z. Jia, S. Liu, T. Xia, L. Peng, Upgraded cellulose and xylan digestions for synergistic enhancements of biomass enzymatic saccharification and bioethanol conversion using engineered *Trichoderma reesei* strains overproducing mushroom LeGH7 enzyme, Int. J. Biol. Macromol. 278 (2024) 134524, https://doi.org/10.1016/j.ijbiomac.2024.134524.
[35] T. Li, H. Peng, B. He, C. Hu, H. Zhang, Y. Li, Y. Yang, Y. Wang, M.M.A. Bakr, M. Zhou, L. Peng, H. Kang, Cellulose de-polymerization is selective for bioethanol refinery and multi-functional biochar assembly using brittle stalk of corn mutant, Int. J. Biol. Macromol. 264 (2024) 130448, https://doi.org/10.1016/j.ijbiomac.2024.130448.
[36] C. Xu, J. Zhu, H. Yu, H. Yu, Y. Yang, Q. Fu, D. Zhan, Y. Wang, H. Wang, Y. Zhang, T. Li, M.M. El-Sheekh, L. Peng, T. Xia, Recyclable cascading of arsenic phytoremediation and lead removal coupled with high bioethanol production using desirable rice straws, Biochem. Eng. J. 168 (2021) 107950, https://doi.org/10.1016/j.bej.2021.107950.
[37] J.x. Yu, L.y. Wang, R.a. Chi, Y.f. Zhang, Z.g. Xu, J. Guo, Adsorption of Pb^{2+}, Cd^{2+}, Cu^{2+}, and Zn^{2+} from aqueous solution by modified sugarcane bagasse, Res. Chem. Intermed. 41 (3) (2015) 1525–1541, https://doi.org/10.1007/s11164-013-1290-1.
[38] K.L. Yu, X.J. Lee, H.C. Ong, W.H. Chen, J.S. Chang, C.S. Lin, P.L. Show, T.C. Ling, Adsorptive removal of cationic methylene blue and anionic Congo red dyes using wet-torrefied microalgal biochar: equilibrium, kinetic and mechanism modeling, Environ. Pollut. 272 (2021) 115986, https://doi.org/10.1016/j.envpol.2020.115986.
[39] G. Yang, L. Wu, Q. Xian, F. Shen, J. Wu, Y. Zhang, Removal of Congo red and methylene blue from aqueous solutions by vermicompost-derived biochars, PloS One 11 (5) (2016) e0154562, https://doi.org/10.1371/journal.pone.0154562.
[40] S.P. Dubey, K. Gopal, Adsorption of chromium(VI) on low cost adsorbents derived from agricultural waste material: a comparative study, J. Hazard. Mater. 145 (3) (2007) 465–470, https://doi.org/10.1016/j.jhazmat.2006.11.041.
[41] D.C. Sharma, C.F. Forster, A preliminary examination into the adsorption of hexavalent chromium using low-cost adsorbents, Bioresour. Technol. 47 (3) (1994) 257–264, https://doi.org/10.1016/0960-8524(94)90189-9.
[42] P.K. Sharma, S. Ayub, C.N. Tripathi, Isotherms describing physical adsorption of Cr (VI) from aqueous solution using various agricultural wastes as adsorbents, Cogent Eng. 3 (1) (2016) 1186857, https://doi.org/10.1080/23311916.2016.1186857.
[43] W. Zheng, X.S.B. Li, F. Wang, Q. Yang, P. Deng, G.m. Zeng, Adsorption removal of cadmium and copper from aqueous solution by areca - a food waste, J. Hazard. Mater. 157 (2) (2008) 490–495, https://doi.org/10.1016/j.jhazmat.2008.01.029.
[44] U. Kumar, M. Bandyopadhyay, Sorption of cadmium from aqueous solution using pretreated rice husk, Bioresour. Technol. 97 (1) (2006) 104–109, https://doi.org/10.1016/j.biortech.2005.02.027.
[45] F.W. Sousa, A.G. Oliveira, J.P. Ribeiro, M.F. Rosa, D. Keukeleire, R.F. Nascimento, Green coconut shells applied as adsorbent for removal of toxic metal ions using fixed-bed column technology, J. Environ. Manage. 91 (8) (2010) 1634–1640, https://doi.org/10.1016/j.jenvman.2010.02.011.
[46] M.S. Kim, J.G. Kim, Adsorption characteristics of spent coffee grounds as an alternative adsorbent for cadmium in solution, Environments 7 (4) (2020) 24, https://doi.org/10.3390/environments7040024.
[47] S. Gu, C.Q. Lan, Effects of culture pH on cell surface properties and biosorption of Pb(II), Cd(II), Zn(II) of green alga *Neochloris oleoabundans*, Chem. Eng. J. 468 (2023) 143579, https://doi.org/10.1016/j.cej.2023.143579.
[48] D. Yoon, Y.W. Son, H. Cheong, Negative thermal expansion coefficient of graphene measured by raman spectroscopy, Nano Lett. 11 (8) (2011) 3227–3231, https://doi.org/10.1021/nl201488g.
[49] S. Roscher, R. Hoffmann, O. Ambacher, Determination of the graphene–graphite ratio of graphene powder by Raman 2D band symmetry analysis, Anal. Methods 11 (9) (2019) 1224–1228, https://doi.org/10.1039/C8AY02619J.
[50] A.C. Ferrari, D.M. Basko, Raman spectroscopy as a versatile tool for studying the properties of graphene, Nat. Nanotechnol. 8 (4) (2013) 235–246, https://doi.org/10.1038/nnano.2013.46.